Research Article

Journal of Environmental Nanotechnology

Nano-structured Molybdenum Trioxide Nano-hybrid based Conductive Platform for Breast Cancer Detection

N. Bharatha Devi[1*], B. Satyasri[2], R. Ramya[3], R. Kanmani[4] and G. Vinuja[1]

[1]Department of Computer Science and Engineering, Saveetha School of Engineering, Saveetha Institute of Medical and Technical Sciences, Saveetha University, Chennai, TN, India

[2]Department of ECE, Vel Tech Rangarajan Dr. Sagunthala R&D Institute of Science and Technology, Avadi, Chennai, TN, India

[3]Department of Nano Electronics Materials and Sensors, Saveetha School of Engineering, Saveetha Institute of Medical and Technical Sciences, Saveetha University, Chennai, TN, India

[4]Department of ECE, SNS College of Technology, Coimbatore, TN, India

Received: 16.04.2024 Accepted: 30.06.2024 Published: 30.06.2024

*bharathi.actech@gmail.com

ABSTRACT

A recently published study describes the use of an electrochemical biosensor that employs a nanohybrid of MoO3. This hybrid material is synthesized using a one-pot hydrothermal process. NH2-functionalized multi-walled carbon nanotubes (MWCNTs) are renowned for their exceptional electrical characteristics, modest surface area, and fast electron transport capacities. The combination of MoO3 and NH2-MWCNTs produces an advanced immune sensing platform that improves the electrochemical performance and sensitivity in detecting HER-2. The Scanning Electron Microscopy (SEM) analysis of the synthesized nanocomposite demonstrates the presence of nanorods enveloped by slender MWCNT fibers, resulting in the creation of a compact network. The addition of NH2-MWCNTs greatly enhances electron transfer, resulting in a tenfold increase compared to pristine MoO_3, which has an average surface area of 63 $m^2\ g^{-1}$. The biosensor has exceptional sensitivity, approximately 26 A $ng^{-1}\ cm^{-2}$ per decade, over a dynamic linear range of 10^{-6} to 10^3 ng mL^{-1}. Additionally, it retains its effectiveness for around five weeks when maintained at a temperature of 4 °C. This immunological sensing platform utilizes anti-HER-2 antibodies to identify the presence of HER-2. Therefore, the MoO3 composite exhibits outstanding electrochemical performance, similar to APTES/MoO3 and APTES/MoO_3@RGO (Reduced Graphene Oxide) electrodes. It has the potential to be used as a matrix for immunological sensing to identify various cancer biomarkers.

Keywords: Nanomaterials; Breast cancer; Biomarkers; Molybdenum trioxide.

1. INTRODUCTION

Cancer is a significant global health concern, characterized by the uncontrolled growth and spread of abnormal cells. These cells can invade neighbouring tissues and metastasize, causing severe complications. Cancer often arises from genetic mutations that disrupt normal cellular regulation, leading to uncontrolled cell growth and division (Spagnolie, 2015). Risk factors include genetic predisposition, lifestyle choices, viral infections, and environmental exposures. Among the numerous types of cancer, breast cancer is notably prevalent, especially among women (Fu *et al*. 2018). Early detection and treatment significantly improve survival rates, with various diagnostic methods available, including non-invasive screening and invasive biopsies.

Nanomaterials have demonstrated a high level of interest in the fields of physical, chemical, and biological systems. Nanomaterials, particularly molybdenum trioxide (MoO_3), have garnered significant interest due to their unique physical, chemical, and electronic properties. Nanostructured MoO_3 (Al-Kattan *et al*. 2016), with its high electrical conductivity, tunable band gap, and high catalytic activity, is recognized for its potential in various applications such as electrochromic systems (Shchegolkov *et al*. 2021), energy storage units, superconductors, thermal materials, and biological sensors (Nazari *et al*. 2021). MoO_3 exists in three crystalline forms: monoclinic (α-MoO_3), orthorhombic (β-MoO_3), and hexagonal (h-MoO_3) (Li *et al*. 2022), each with unique structural characteristics that contribute to its functionality. These phases are generated by the corner-sharing oxygen atoms in the MoO_6 octahedron, which is held together by covalent forces and has a distinct layered structure. This is represented in Fig. 1. The six oxygen atoms surrounding the Mo atom in the centre result in layers bonded *via* van der Waals force. h-MoO_3 is the most stable phase, with great intercalation capacity and increased Mo^{6+}/Mo^{4+} redox activity.

Cellular regulatory inadequacies from genetic damage cause most cancers. In general, genes control cell growth and reproduction (Casais-Molina *et al*. 2018). Normal gene regulation can be disrupted by mutation during cell division. Mutations affect cancer cell metabolism, growth, proliferation, and death. The cause of cancer is unknown, however family history, lifestyle, virus exposure, and environmental dangers contribute.

Breast, liver, stomach, lung, and skin cancers are among nearly 200 types (Ferlay *et al*. 2020). Breast cancer is the most common malignancy in women and curable in 70–80% of early-stage patients (Watkins, 2019). It causes 11.6% of female malignancies and 22.9% of invasive cancers, killing 627,000 women in 2018. Screening and self-examination can detect breast cancer, followed by a biopsy (Waks and Winer, 2019). Biomarkers are quantitative indicators of biological states, activities, or conditions (Schneider *et al*. 2009), pathogenic processes, or treatment responses (Paczesny *et al*. 2015). Biomarkers, biological entities in body fluids, can diagnose diseases, including cancer. Disease is indicated by abnormal biomarkers. Using MoO3's unique features in biosensor technology could lead to early and accurate breast cancer detection, advancing cancer diagnosis (Zadan *et al*. 2021).

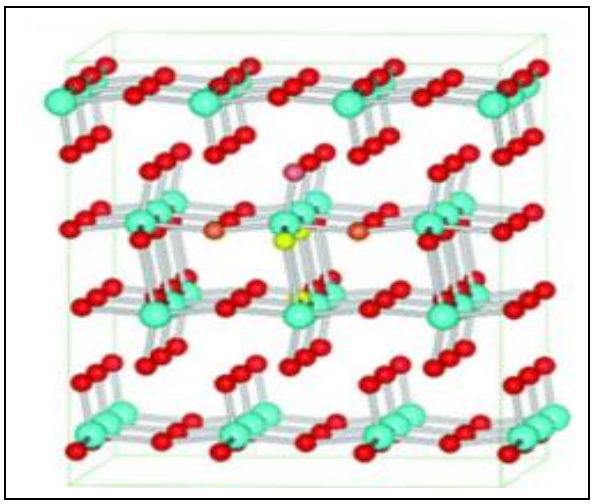

Fig. 1: Crystal structure of orthorhombic MoO_3 showing the layered structure

This study focuses on developing an electrochemical immunosensor for cancer detection with a simple manufacturing approach, enhanced sensitivity, and improved limit of detection (LOD), specifically targeting HER-2, a breast cancer biomarker. The goal is to create a highly sensitive, label-free, biocompatible biosensing system using nanostructured MoO_3. Key steps involve synthesizing and characterizing nanostructured MoO_3, fabricating the immunoelectrode through electrochemical deposition, and immobilizing antibodies onto the fabricated surface. Preliminary results indicate that the Bovine Serum Albumin/anti-HER-2/MoO_3/Indium Tin Oxide immune electrode can efficiently detect the HER-2 biomarker, showing promise for clinical applications (Ramakrishnan *et al*. 2019).

2. LITERATURE REVIEW

Prakash *et al*. (2019) described the production of MoO_3 nanorods for use in electrochemical supercapacitors. Investigated MoO_3 and MoO_3 nanostructures in another work. It was established that the sensing of hydrogen gas employing MoO_3 displayed improved sensing and charge transfer due to its layered structure (Qiao *et al*. 2019). Chiew *et al*. (2021) evaluated the catalytic property of MoO_3. They reported the influence of ring-opening oxides and amines on the catalytic action of MoO_3. Investigated the potential of MoO_3 as high-rate electrochemical anodes for dual ion intercalation energy storage devices using the interlayer gap widening process. The ionic channel is expanded when the interlayer gap widens, resulting in better and enhanced electrochemical kinetics.

Chen *et al*. (2008) explored the selective sensing mechanism of MoO_3 towards diverse biomolecules using simulations. The role of surface imperfections in the oxide was explored during contact with various molecules. The research sheds light on the application of MoO_3 as an ultrasensitive and ultra-selective material in the fabrication of sensing devices. The use of MoO_3 in the field of biomedical engineering has lately increased due toits availability in various oxidation states. Uyan, (2022) MoO_3 is essentially used as a transducing element in biological applications. When surrounded by oxygen vacancies in the lattice, the Mo^{6+} atom tends to decrease to the Mo^{5+} state, moving single electron to the conduction band and resulting in improved conductivity (Malik *et al*. 2022). The study presented an electrical sensor based on MoO_3 using bovine serum albumin as the protein of interest. Two-dimensional nanoflakes were used to create a conduction channel with a shorter response time. (Yang *et al*. 2021) explored the revolutionary MoO_3 nanoflakes in the field of bio mimicking. A two-dimensional three-terminal synaptic transistor simulating the neural synapse has been developed (Cheng and Compton, 2014) A recent work described the MoO_3-x flakes employing visual measurement of glucose with oxygen deprived glucose oxidase (Madhavi *et al*. 2023).

It should be noted that the electrochemical use of MoO_3 may be substantially hampered due to its poor electrochemical kinetics as well as low charge transfer capability (Cheng and Compton, 2014). To address such issues, doping and compositing molybdenum oxides with various organic materials may result in improved material specific features and a widening of its use to highly efficient electrochemical systems, biocatalysts, and biosensing units (Barabash *et al*. 2020). The limitations created by the pristine nanomaterial are solved by a nanohybrid formed by the mixture of organic and inorganic nanomaterials (Malathi *et al*. 2024). The existing study discovered that nanohybrids of MoO_3 with carbonaceous materials such as MWCNT and RGO result in increased heterogeneous electron transport, quicker

electron kinetics, a large surface area, and improved biosensing characteristics (Tan *et al*. 2016).

3. EXPERIMENTAL WORK

3.1 MoO_3 Nano-hybrid based Conductive Platform for Breast Cancer Detection

3.1.1 In Situ Synthesis of MoO_3 Nanocomposite

Carbon nanotubes (CNTs) have received the major attention as a material of interest in the ever-growing field of point-of-care devices because of their high conductivity, exceptional stability and thermal properties. The MWCNTs have superior electronic properties, compound inertness, electric stability, large specific surface area, as well as mechanical properties. Thus, they are promising candidates for use in a variety of applications including, gas sensing, power storage, strain sensing and biosensing.

The MoO_3 nanocomposite was fabricated using a one-pot hydrothermal technique. In 20 mL deionized water (DI), a solution of NH_2-MWCNT (0.2 g) was ultrasonicated for 30 minutes (solution B; Fig. 2).

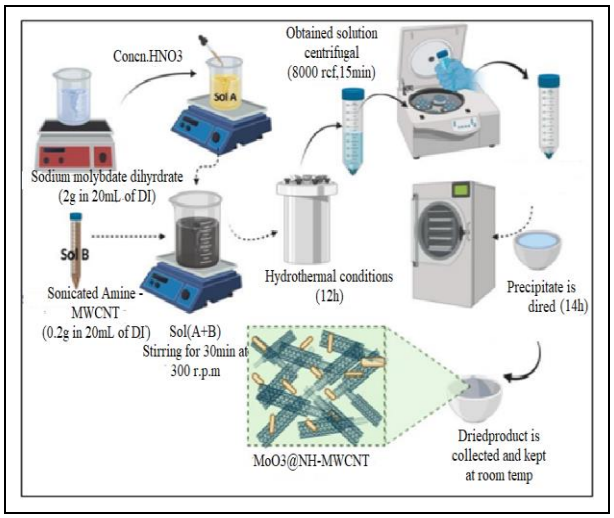

Fig. 2: In situ synthesis of MoO_3 nanocomposite

Simultaneously, a solution A was prepared by dissolving 2 g of $Na_2MoO_4.2H_2O$ in 20 mL of DI and stirring at 300 rpm for 1 hour at room temperature (25°C). Following that, 5 mL of $HNO_3$was added dropwise to solution B until the solution became light yellow and the pH reached 2. The mixture was agitated for another 30 minutes to ensure homogeneity (Salari and Hosseini, 2021). The entire solution was placed in a 100 mL Teflon-coated stainless steel autoclave, where it was sterilized for 14 hours at 180°C. Then, the homogeneous solution was collected and rinsed with DI water until the pH was neutral. The resulting product was collected in a crucible and dried overnight at 60°C. Once the powder had completely dried, it was collected and stored anhydrous until further use.

3.2 Fabrication of MoO_3 based Electrodes

The as-prepared MoO_3nano composite was electrophoretically placed over a hydrolyzed ITO glass substrate. For this, a homogenous MoO_3 solution in acetonitrile (1 mg mL^{-1}) was prepared. To minimize overheating surrounding the sample, the solution was sonicated for roughly 30 minutes at 5-minute intervals. About 10 mL of colloidal solution was added to a glass cell with platinum (Pt) serving as counter electrode and ITO serving as working electrode. For the movement of suspended nanoparticles to create uniform thin films on the ITO substrate, an external DC voltage of 55 V was supplied for 1.30s using an electrophoretic deposition device (0.25 cm^2). To remove the loosely attached nanoparticles, the produced films (MoO_3/ITO) were air dried and washed with DI water. Similarly, many sets of electrodes were fabricated and kept at ambient temperature (25°C).

3.3 Fabrication of MoO_3 Nano Composite based Immune Sensor

Before being poured onto electrodes, a mixture of 15 L of anti-HER-2 (50 g mL^{-1}), 7.5 L of EDC (0.4 M), and 7.5 L of NHS (0.1 M) was prepared and kept at room temperature (25°C) for 30 minutes (Fig. 3).

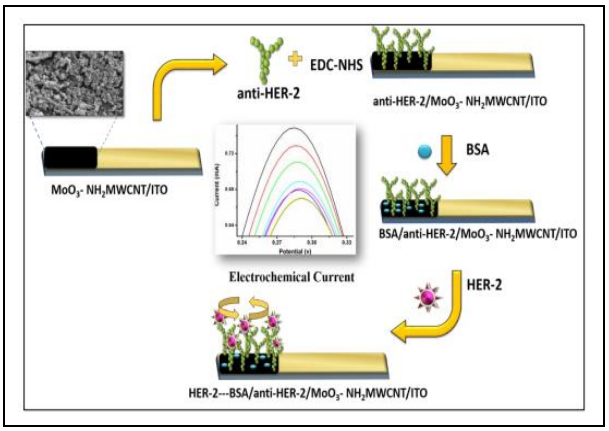

Fig. 3: Fabrication of MoO_3 nanocomposite based immunosensor

Following that, 30 L of this produced solution was drop cast evenly over the MoO_3/ITO electrode and kept humid for 4-5 hours. During this time, a covalent contact occurred between the -COOH group on the Fc region of anti-HER-2 and the -NH_2 group of MoO_3 nanocomposites, resulting in the formation of an amide bond. After that, the electrode was washed in phosphate buffer solution (PBS)to get rid of any unattached biomolecules before being given 20 L BSA (1 mg mL^{-1}) to block all active sites. The immunological electrode

was then cleaned with PBS buffer and stored at 4 °C for future use.

4. RESULTS AND DISCUSSION

The MoO_3 and the NH_2-MWCNTs (Fig. 4) were subjected to XRD analyses in 10-80° range at scan rate of 0.2° min^{-1} to determine their crystalline structure. The diffraction pattern obtained for the MoO_3 nanocomposite is consistent with the orthorhombic phase of MoO_3 (JCPDS number: 89-5108), with strong intensity peaks occurring at 2θ = 12.8°, 23.4°, 25.7°, 27.5°, and 38.9°, corresponding to the hkl planes (020), (110), (120), (021) and (020), respectively (060). Strong crystalline nature is confirmed by the clearly defined peaks in XRD pattern, which has lattice constants (a = 3.9, b = 13.8, and c = 3.7) and space group PNMA. Because the distinctive peak of MWCNTs at 26.0° (040) clashes with the high intensity peak of MoO_3 (120) in the nanocomposite, no separate MWCNT peak was seen. The high crystalline structure of the as-synthesized nanocomposite indicates that MoO_3 nanorods develop anisotropically in the nanocomposite.

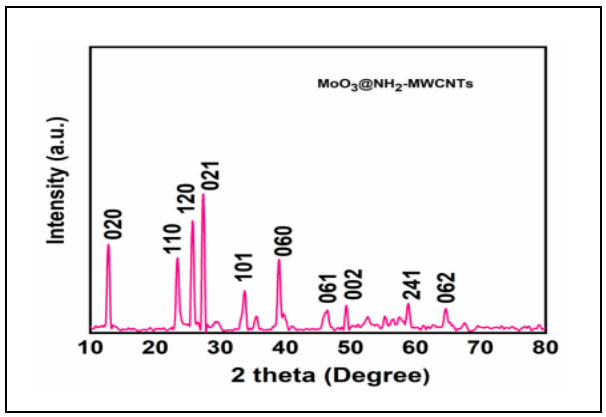

Fig. 4: XRD spectra of as-synthesized MoO_3 nanocomposite

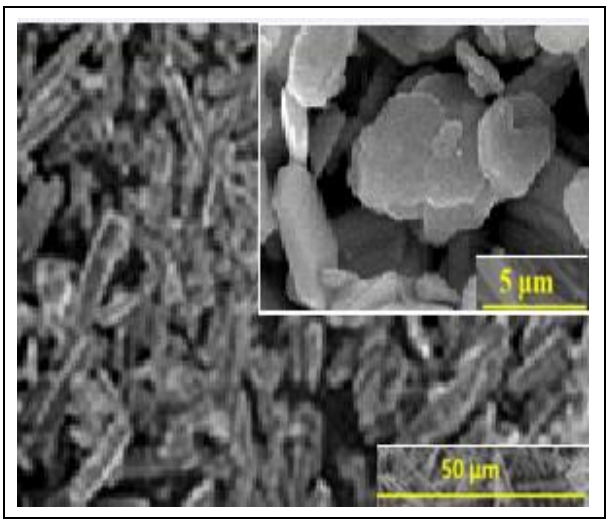

Fig. 5: The SEM image of synthesized $nMoO_3$

4.1 Scanning Electron Microscopy

Scanning electron microscopy was used to study the morphology of synthesized $nMoO_3$ (Fig. 5). It shows microscopic needle-like formations. The magnified image reveals rod-like structure of $nMoO_3$.

4.2 Transmission Electron Microscopy (TEM)

Transmission electron microscopy was used to characterize the morphology of the synthesised $nMoO_3$. It shows the formation of rod-like $nMoO_3$ structures with diameter range 60 to 80 nm and length of few µm.

4.3 Raman Spectroscopic Studies

The Raman spectra of the produced $nMoO_3$ nanorods are shown in Fig. 6. It is possible that high intensity surface morphology at 818.2 cm^{-1} is caused by stretch modes of doubly linked bridge oxygen ions in Mo-O-Mo that are present in the MoO_6 octahedrons.

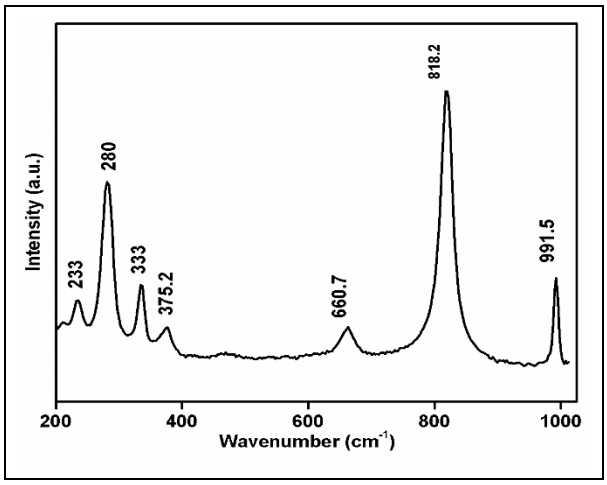

Fig. 6: Raman Spectra for the nMoO3

The peak at 991.5 cm^{-1} shows that terminal oxygen in Mo=O experiences an asymmetric stretching phase. The peak at 280 cm^{-1} is a doublet of wriggling modes displayed by terminal oxygen atoms. The peak at 660.7 cm^{-1} might be explained by triple-coordinated oxygen atoms connected to the Mo-O stretching modes of triple octahedra. Its O=Mo=O bending and scissoring modes, respectively, were attributed to the peaks measured at 333 and 375.2 cm^{-1}.

4.4 Brunauer Emmett Teller study

Brunauer Emmett Teller tests were used to determine the exact surface area and porosity of the synthesised $nMoO_3$. The model was degassed in a vacuum at 200 °C for two hours to calculate its specific surface area, and nitrogen desorption and adsorption isotherms were recorded. The BET tests revealed that the overall pore volume of $nMoO_3$ was 0.029 cc g^{-1}. The

specific surface area of $nMoO_3$ was determined to be 17.19 m^2 g^{-1} by the BJH technique. According to the pore size curve, mesoporous $nMoO_3$ predominated, with microporous $nMoO_3$ accounting for a minor percentage of the material. The average pore thickness was found to be 6.8 nm. The obtained results suggested that the synthesised $nMoO_3$ has a highly mesoporous characteristic, which allows for increased anti-HER-2 loading.

4.5 X-ray Photoelectron Spectroscopic (XPS)

The survey scanXPS spectra for APTES/$nMoO_3$and anti-HER-2/APTES/$nMoO_3$ onto ITO electrode are shown in Fig. 7. Peaks were found near 232, 102, 530.5, and 399.6 eV, respectively, for Mo 3d, Si 2p, O 1s, and N 1s.

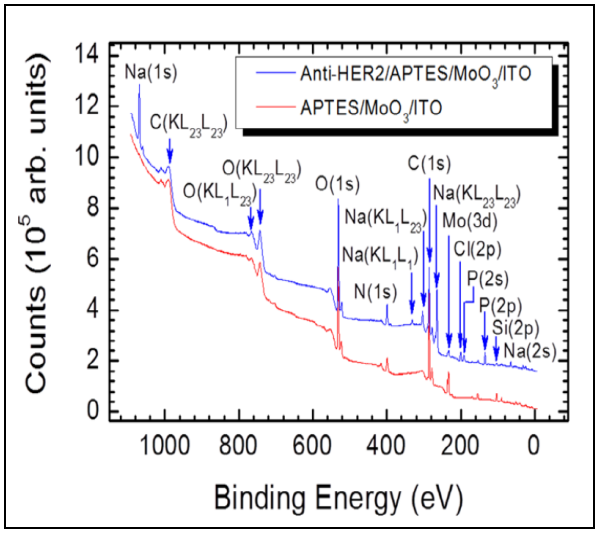

Fig. 7: Survey scan XPS spectra of $nMoO_3$ and anti-HER-2/APTES/$nMoO_3$/ITO electrode

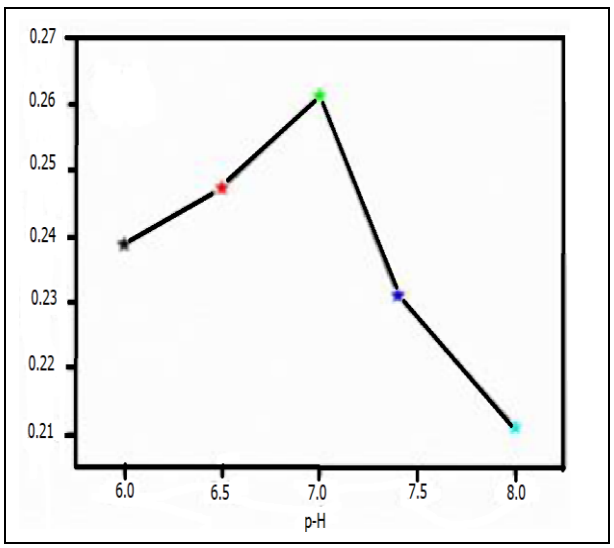

Fig. 8: Effect of different pH (6.0 to 8.0) on the fabricated immunoelectrode

4.6 pH and Electrode Studies

The effect of pH (6.0-8.0) on BSA/anti-HER-2/APTES/$nMoO_3$/ITO immunoelectrode was examined using DPV in PBS buffer containing 5mM of $[(Fe(CN)_6)]^{3-/4-}$ ions. Highest current response observed at pH 7.0 is shown in Fig. 8. This is because biomolecules, including as DNA, mRNA, enzymes, antibodies, and antigens exist in their specific shapes and experience their highest bio-molecular mobility at pH 7.0. However, interactions using H^+ or OH^- ions within amino acid sequence of the antibodies may have caused the biomolecules to get denatured in acidic or basic solution.

4.7 Cyclic Voltammograms Studies

Differential pulse voltammetry tests were conducted in the potential window of -0.2 to +0.6 V, as shown in Fig. 9. The peak current generated for APTES/$nMoO_3$/ITO (0.31 mA) was discovered to be higher than that of ITO due to strong electrocatalytic efficiency and large surface area of $nMoO_3$ nanorods (0.20 mA). Anti-HER-2 antibodies immobilized caused the current value to decrease to 0.24 mA and 0.23 mA, respectively. This decrease was attributable to the insulating properties of BSA and anti-HER-2, which worked to prevent free electron transfer to the immunoelectrode.

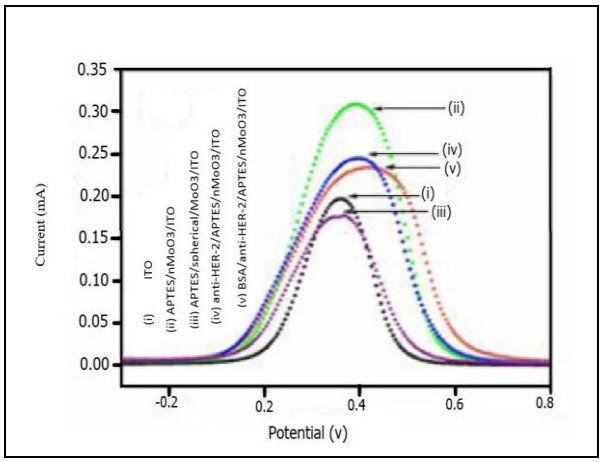

Fig. 9: Electrode studies at different steps of modification of the electrode

4.8 Structural and Morphological Analysis

The SEM scans were used to analyze the morphology of the as-synthesized MoO_3 nanocomposite. Nanorods of virgin MoO_3 nanoparticles were formed randomly and densely. The average size of the produced MoO_3 nanorods was determined to be approximately 150 nm to a few microns. The NH_2- MWCNTs are entirely wrapped around MoO_3 nanorods to produce an interwoven structure. The crystalline MoO_3 nanorods are interlaced with -NH_2-MWCNTs nanofibers, resulting in

the development of a forest-like network. The structural and morphological analysis results are shown in Figs. 10, 11 and 12.

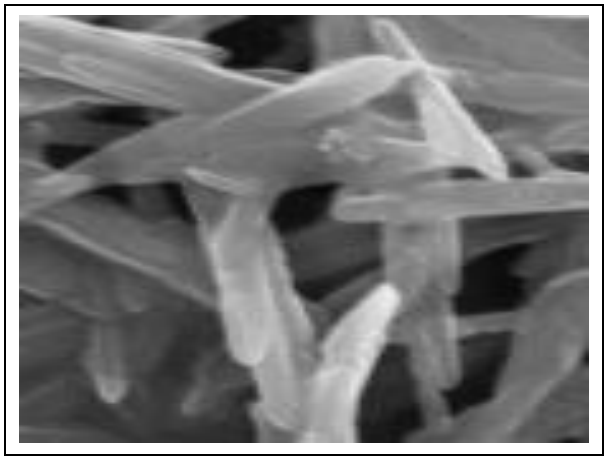

Fig. 10: SEM image of the as-synthesized nano composite

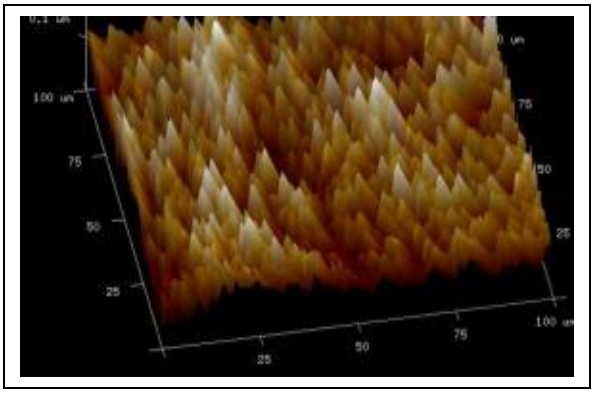

Fig. 11: MoO_3@/ITO

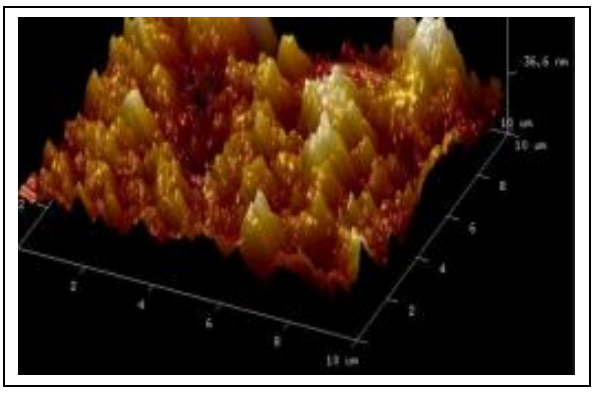

Fig. 12: Anti-HER-2/MoO3@NH_2-MWCNTs/ITO electrodes

The MoO_3/ITO and anti-HER2/MoO_3/ITO electrodes were subjected to FT-IR experiments to determine the presence of the functional groups and surface modification in the 4000–400 cm^{-1} range shown in Figs. 5 and 6. The symmetric stretching of Mo-O of MoO_3 with in orthorhombic phase and terminal stretching vibration of Mo=O are responsible for the two peaks on spectrum (a) & (b) at 900 cm^{-1} and 688 cm^{-1}, respectively. The band at 1080 cm^{-1} was attributed to C-N stretching. The N-H scissoring for plane bending mode, N-H deformation of primary -NH_2 group present here on surface of MoO_3 nanocomposite are also responsible for peaks at 1640 $cm^{-1}$and 3370cm^{-1}, respectively.

The -CH stretching of nanocomposites is related to an appearance of elusive peak at 2730-2977 cm^{-1}. Spectrum (b) shows peaks at 1700 cm^{-1} and 1382 cm^{-1}, along with a faint peak at 1158 cm^{-1} due to C-O (ester) vibrations, which combined with presence of peaks at 1700 cm^{-1} and 1382 cm^{-1} indicating amide bond intercalated between free -NH_2 groups of MoO_3 nanocomposite and -COOH group of anti-HER2 antibodies. In Fig. 13, the comparison is displayed.

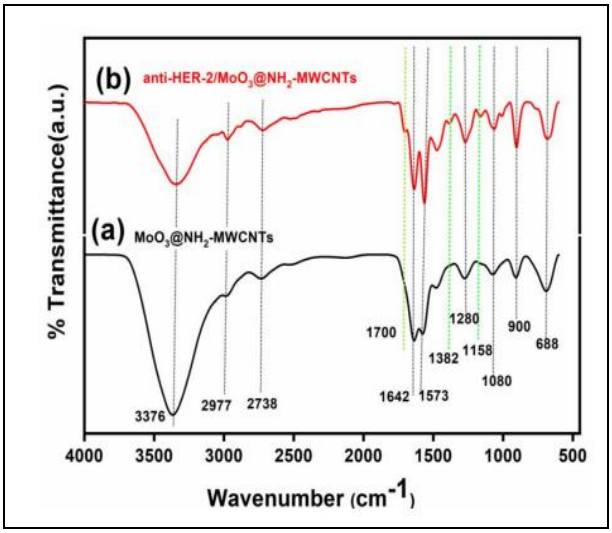

Fig. 13: FTIR spectra of (a) MoO_3@NH_2-MWCNTs/ITO, (b) anti-HER-2/MoO_3@NH_2- MWCNTs/ITO electrodes

Using DPV in the presence of different pH ranging from 0 to 10, the impact of pH on electrochemical reactivity of BSA/anti-HER-2/MoO_3/ITO electrodes was investigated. The largest current response was at pH 7.0-7.5, while Fig. 14 shows a slightly higher value at pH 7.0. (a). This response may be due to the fact that biomolecules prefer to maintain their natural activity near neutral pH values, but interactions with H^+ or OH^- ion at acidic and basic pH tend to denature these antibodies. Incubation studies were done to find out how long an immune electrode's anti-HER-2 antibody would associate with HER-2 antigen (b). For this, HER-2 antigen (1 ng mL^{-1}) was administered into electrochemical cell that after immune electrode BSA/anti-HER-2/MoO^3/ITO were immersed in the cell. The DPVs were recorded at five-minute intervals until 30 minutes. It was discovered that the interaction of the HER-2 antigen and antibody complex begins to develop, resulting in a decrease in current owing to the obstruction of electron transport. It was discovered that

the anti-HER-2 antibodies needed 15 minutes to completely bind with the antibodies.

4.9 Control and Selectivity Studies

Electrochemical response of bare APTES/nMoO$_3$/ITO electrode to different doses of HER-2 antigen (2.5-110 ng mL^{-1}) were assessed (Fig. 14) to test the current responsiveness of the proposed sensor. The peak current did not significantly alter, demonstrating that the APTES/nMoO$_3$/ITO electrode didnot produce an artificial electrochemical response. This control experiment showed that the sensor response was purely due to the transmission of anti-HER-2 and HER-2 biomolecules.

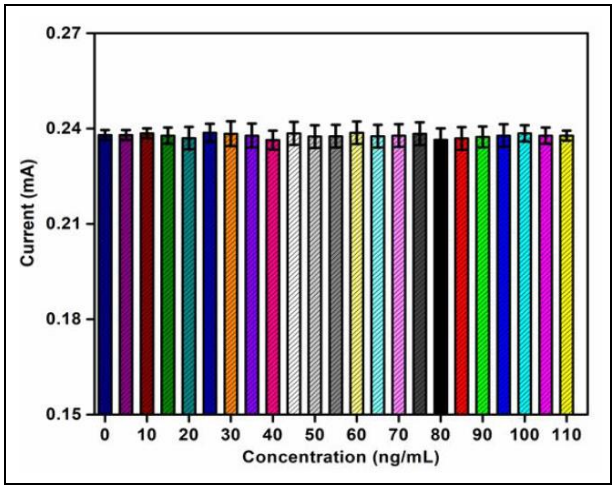

Fig. 14: Control Studies of the APTES/nMoO$_3$/ITO electrode in the presence of HER-2

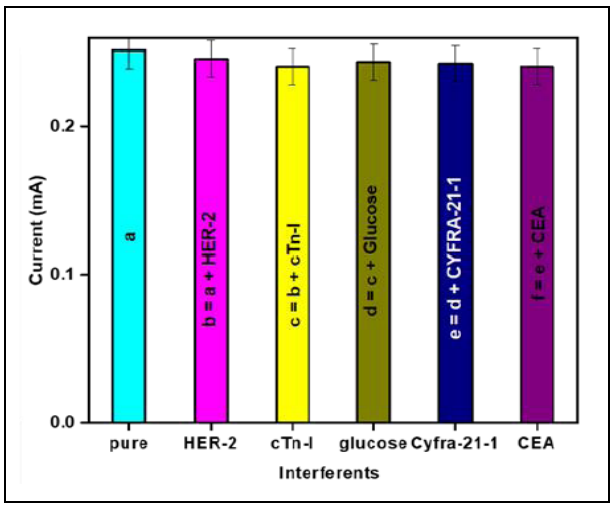

Fig. 15: Selectivity studies of the fabricated immunoelectrode

This could be as a result of protein binding sites folding and opposing one another at low pH, which causes molecules to move further apart. Results demonstrated the potential for at least five regenerations of proposed immunosensors. Differential pulse voltammetry was used to study the selectivity of BSA/anti-HER-2/APTES/nMoO$_3$/ITO immunoelectrodes towards various bimolecular found in blood samples of breast cancer patients (Fig. 15).

4.10 Electrochemical Recognition of the Cancer Biomarker

Using DPV technique in the potential range -0.2 to +0.6 V, electrochemical reaction experiments of its BSA/anti-HER-2/APTES/nMoO$_3$/ITO immunoelectrode were conducted in PBS (pH 7.0) adding 5 mM [Fe (CN)^6]3-/4-] as shown in Fig. 16 (a and b). For each concentration of HER-2, each measurement was carried out three times (n = 3). It was discovered that anodic peak current decreased in line with the rise in HER-2 levels. The interaction of anti-HER-2 with HER-2 specific binding sites caused dielectric antigen-antibody complex molecules to form at the transducer surface, leading to a decrease in response current.

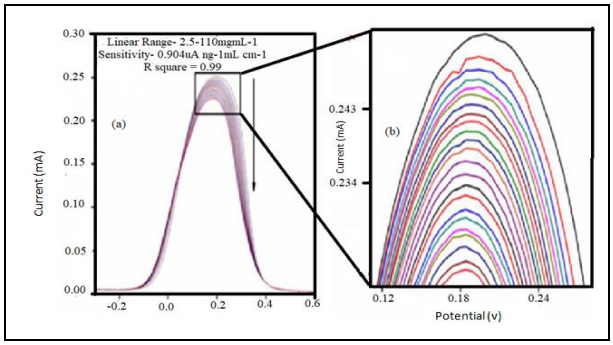

Fig. 16: (a)Electrochemical response of the BSA/anti-HER-2/APTES/nMoO$_3$/ITO immune electrode as a function of HER-2 concentration using DPV(b) The magnified view of oxidation peak current

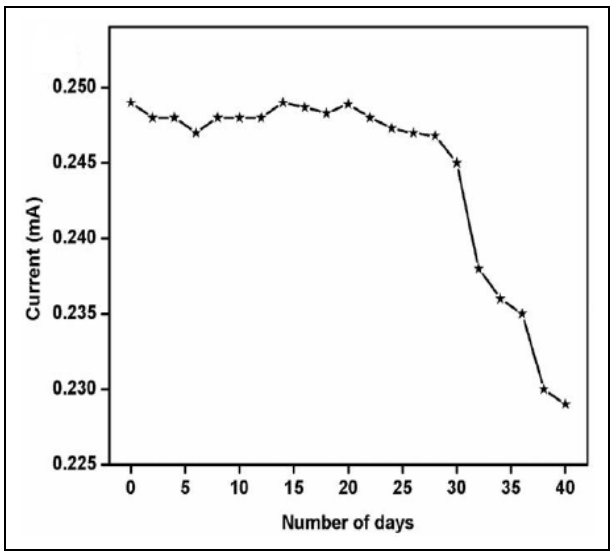

Fig. 17: Shelflife study of BSA/anti-HER-2/APTES/ nMoO$_3$/ITO immunoelectrode

4.11 Shelf-Life Studies

The clinical accuracy of the developed immunosensor was tested using five blood samples from a breast cancer patients. Following that, its HER-2 levels were determined using an ELISA using a double sandwich. Fig. 17 shows that an adequate proportion of relative standard deviation (% RSD) and correlation were obtained. The results showed that the developed immunosensor has a very high sensitivity for detecting HER-2 in clinical specimens.

5. CONCLUSION

A highly sensitive electrochemical immune-sensor based on MoO_3, a conducting material nanocomposite, for assessment of the breast cancer using biomarker HER-2 was developed. Growth of MoO_3 on the NH_2-MWCNTs fibres formed a robust linked mesh-like network. The specific surface area assessed by BET tests was 63 m^2 g^{-1} with pore sizes ranging from 2 to 50 nm, showing the presence of mesoporous structures, which contributes to the extraordinary sensitivity and outstanding durability of immunosensors. Additionally, it was discovered that HET ratio of nanocomposites was 9.6 times higher compared to virgin MoO_3. The synthesized nanocomposite was electrophoretically coated onto an ITO substrate and then immobilized with anti-HER-2. With a sensitivity of 26 A ng^{-1} cm^{-2} and a tolerable stability of 35 days, this immune electrode, which consists of BSA/anti-HER-2/MoO_3/ITO, was shown to be linear in the range 10^6 to 10^3 ng mL^{-1}. Improved heterogeneous electron transfers with higher biomolecular loading in this nanocomposite have led to a wider linear detection range, exceptional sensitivity, and detection limits as low as 10^{-6} ng mL^{-1}. According to the real sample findings, the novel BSA/anti-HER-2/MoO_3/ITO immune electrode may effectively detect HER-2 biomarker and has a bright future in terms of its clinical applicability.

AUTHORS CONTRIBUTIONS

N. Bharatha Devi, B. B. Beenarani and V. R. Balaji were major contributors in writing the manuscript.

R. Ramya and G. Vinuja analyzed and interpreted the data regarding the secure route finding.

All authors read and approved the final manuscript.

FUNDING

There is no funding source.

CONFLICT OF INTEREST

The authors declared no conflict of interest in this manuscript regarding publication.

AVAILABILITY OF DATA AND MATERIALS

We recognize it is not always possible to share research data publicly, for instance when individual privacy could be compromised, and in such instances data availability should still be available in the manuscript.

COPYRIGHT

This article is an open-access article distributed under the terms and conditions of the Creative Commons Attribution (CC BY) license (http://creativecommons.org/licenses/by/4.0/).

REFERENCES

Al-Kattan, A., Ryabchikov, Y.V., Baati, T., Chirvony, V., Sanchez-Royo, J.F., Sentis, M., Braguer, D., Timoshenko, V.Y., Esteve, M.A. and Kabashin, A.V., Ultrapure laser-synthesized Si nanoparticles with variable oxidation states for biomedical applications. *J. Mater. Chem.*, 4(48), 7852-7858 (2016). https://doi.org/10.1039/C6TB02623K

Barabash, D., Barabash, A., & Pinaev, S., Radiation Resistant Composite for Biological Protection of the Personnel, *Arch Tech Sci.*, 2(23), 67–76 (2020). https://doi.org/10.7251/afts.2020.1223.067B

Casais-Molina, M.L., Cab, C., Canto, G., Medina, J. and Tapia, A., Carbon nanomaterials for breast cancer treatment, *J. Nanomater.*, 1-9 (2018). https://doi.org/10.1155/2018/2058613

Chen, W., Nanoparticle fluorescence based technology for biological applications, *J. Nanosci. Nanotechnol.*, 8(3), 1019-1051 (2008). https://doi.org/10.1166/jnn.2008.301

Cheng, W. and Compton, R.G., Electrochemical detection of nanoparticles by 'nano-impact'methods, *TrAC, Trends Anal. Chem.*, 58, 79-89 (2014). https://doi.org/10.1016/j.trac.2014.01.008

Chiew, C., Morris, M.J. and Malakooti, M.H., Functional liquid metal nanoparticles: synthesis and applications, *Mater. Adv.*, 2(24), 7799-7819 (2021). https://doi.org/10.1039/D1MA00789K

Ferlay, J., Colombet, M., Soerjomataram, I., Parkin, D.M., Piñeros, M., Znaor, A. and Bray, F., Cancer statistics for the year 2020: An overview, *Int J Cancer.*, 149(4), 778-789 (2021). https://doi.org/10.1002/ijc.33588

Fu, K., Wang, R., Katase, T., Ohta, H., Koch, N. and Duhm, S., Stoichiometric and oxygen-deficient VO_2 as versatile hole injection electrode for organic semiconductors, *ACS Appl. Mater. Interfaces.*, 10(12), 10552-10559 (2018). https://doi.org/10.1021/acsami.8b00026

Li, M., Huang, G., Chen, X., Yin, J., Zhang, P., Yao, Y., Shen, J., Wu, Y. and Huang, J., Perspectives on environmental applications of hexagonal boron nitride nanomaterials, *Nano Today*, 44, 101486 (2022). https://doi.org/10.1016/j.nantod.2022.101486

Madhavi, M., Sasirooba, T. and Kumar, G. K., Hiding Sensitive Medical Data Using Simple and Pre-Large Rain Optimization Algorithm through Data Removal for E-Health System, *J. Internet Serv. Inf. Secur.*, 13, 177-192. (2023). https://doi.org/10.58346/JISIS.2023.I2.011

Malathi, K., Shruthi, S.N., Madhumitha, N., Sreelakshmi, S., Sathya, U. and Sangeetha, P.M., Medical Data Integration and Interoperability through Remote Monitoring of Healthcare Devices, *J. Wirel. Mob. Netw. Ubiquitous Comput. Dependable Appl.*, 15(2), 60-72 (2024). https://doi.org/10.58346/JOWUA.2024.I2.005

Malik, U., Korcoban, D., Mehla, S., Kandjani, A.E., Sabri, Y.M., Balendhran, S. and Bhargava, S.K.,Fabrication of fractal structured soot templated titania-silver nano-surfaces for photocatalysis and SERS sensing. *Appl. Surf. Sci.*, 594, 153383 (2022). https://doi.org/10.1016/j.apsusc.2022.153383

Nazari, M.A., Maleki, A., Assad, M.E.H., Rosen, M.A., Haghighi, A., Sharabaty, H. and Chen, L., A review of nanomaterial incorporated phase change materials for solar thermal energy storage, *Sol. Energy*., 228, 725-743 (2021). https://doi.org/10.1016/j.solener.2021.08.051

Paczesny, S., Hakim, F.T., Pidala, J., Cooke, K.R., Lathrop, J., Griffith, L.M., Hansen, J., Jagasia, M., Miklos, D., Pavletic, S. and Parkman, R., National Institutes of Health consensus development project on criteria for clinical trials in chronic graft-versus-host disease: III. The 2014 Biomarker Working Group Report, *Biol Blood Marrow Transplant.*, 21(5), 780-792 (2015). https://doi.org/10.1016/j.bbmt.2015.01.003

Prakash, N.G., Dhananjaya, M., Narayana, A.L. and Hussain, O.M., One-dimensional MoO_3/Pd nanocomposite electrodes for high-performance supercapacitors, *Mater. Res. Express*, 6(8), (2019). https://doi.org/10.1088/2053-1591/ab273e

Qiao, J.C., Wang, Q., Pelletier, J.M., Kato, H., Casalini, R., Crespo, D., Pineda, E., Yao, Y. and Yang, Y., Structural heterogeneities and mechanical behavior of amorphous alloys, *Prog. Mater. Sci.*, 104, 250-329 (2019). https://doi.org/10.1016/j.pmatsci.2019.04.005

Ramakrishnan, J., Ravi Sankar, G., and Thavamani, K., Publication Growth and Research in India on Lung Cancer Literature: A Bibliometric Study, *Indian Journal of Information Sources and Services*, 9(S1), 44–47 (2019). https://doi.org/10.51983/ijiss.2019.9.S1.566

Salari, H. and Hosseini, H.H., In situ synthesis of visible-light-driven a-MnO_2 nanorod/AgBr nanocomposites for increased photoinduced charge separation and enhanced photocatalytic activity, *Mater. Res. Bull.*, 133, 111046 (2021). https://doi.org/10.1016/j.materresbull.2020.111046

Schneider, P., Hampel, H. and Buerger, K., Biological marker candidates of Alzheimer's disease in blood, plasma, and serum, *CNS Neurosci. Ther.*, 15(4), 358-374 (2009). https://doi.org/10.1111/j.1755-5949.2009.00104.x

Shchegolkov, A.V., Jang, S.H., Shchegolkov, A.V., Rodionov, Y.V., Sukhova, A.O. and Lipkin, M.S., A brief overview of electrochromic materials and related devices: A nanostructured materials perspective, *J. Nanomater.*, 11(9), 2376 (2021). https://doi.org/10.3390/nano11092376

Spagnolie, S.E., Complex fluids in biological systems. *Bio Med Phy Biomed Eng.*, (2015).

Tan, G.R., Wang, M., Hsu, C.Y., Chen, N. and Zhang, Y., Small upconverting fluorescent nanoparticles for biosensing and bioimaging, *Adv. Opt. Mater.*, 4(7), 984-997 (2016). https://doi.org/10.1002/adom.201600141

Uyan, A. A Review on the Potential Usage of Lionfishes (Pterois spp.) in Biomedical and Bioinspired Applications, *Natural and Engineering Sciences*, 7(2), 214-227 (2022). https://doi.org/10.28978/nesciences.1159313

Waks, A. G. and Winer, E. P. Breast cancer treatment: a review, *Jama*, 321(3), 288-300 (2019). https://doi.org/10.1001/jama.2018.19323.

Watkins, E. J., Overview of breast cancer, *J. Am. Acad. Physician Assist.*, 32(10), 13-17 (2019). https://doi.org/10.1097/01.JAA.0000580524.95733.3d

Yang, W., Wang, L., Mettenbrink, E.M., DeAngelis, P.L. and Wilhelm, S., Nanoparticle toxicology, *Annu. Rev. Pharmacol. Toxicol.*, 61(1), 269-289 (2021). https://doi.org/10.1146/annurev-pharmtox-032320-110338

Zadan, M., Chiew, C., Majidi, C. and Malakooti, M.H., Liquid metal architectures for soft and wearable energy harvesting devices, *Multifunct. Mater.*, 4(1), 012001 (2021). https://doi.org/10.1088/2399-7532/abd4f0